https://doi.org/10.5194/gmd-2019-113
Preprint. Discussion started: 19 August 2019

Geoscientific Model Development Discussions
Open Access
EGU

Using Arctic ice mass balance buoys for evaluation of modelled ice energy fluxes

Alex West[1], Mat Collins[2], Ed Blockley[1]

[1]Met Office Hadley Centre, FitzRoy Road, Exeter EX1 3PB
[2]Centre for Engineering, Mathematics and Physical Sciences, University of Exeter, Stocker Rd, Exeter EX4 4PY

Abstract. Arctic sea ice has declined rapidly over recent decades. Models predict that the Arctic will be nearly ice-free by mid-century, but the spread in predictions of sea ice extent is currently large. The reasons for this spread are poorly understood, partly due to a lack of observations with which the processes by which Arctic atmospheric and oceanic forcing affect sea ice state can be examined. In this study, a method of estimating fluxes of top melt, top conduction, basal conduction and ocean heat flux from Arctic ice mass balance buoy elevation and temperature data is presented. The derived fluxes are used to evaluate modelled fluxes from the coupled climate model HadGEM2-ES in two densely sampled regions of the Arctic, the North Pole and Beaufort Sea. The evaluation shows the model to overestimate the magnitude of summer top melting fluxes, and winter conductive fluxes, results which are physically consistent with an independent sea ice and surface energy evaluation of the same model.

1. Introduction

The climate of the Arctic Ocean region is characterised by the presence of a semi-permanent sea ice cover that acts to reflect solar energy in summer and insulate ocean heat in winter. Arctic sea ice has changed rapidly over the past 30 years, with a decline in extent of 0.84 x 10^6 km^2 per decade observed during the month of September according to the HadISST1.2 dataset (Rayner et al., 2003), and evidence of concurrently declining ice volume (e.g. Rothrock et al., 2008, Lindsay and Schweiger, 2015). Model projections from CMIP5 suggest that the Arctic Ocean is likely to become nearly ice-free in September by mid-century (Massonnet et al, 2012), an event that would have serious implications for the climate (through decreased surface albedo and decreased insulation between the ocean and atmosphere) and for geopolitics. However, these model projections vary greatly in their simulation of the mean state of Arctic sea ice in the present day, as well as the speed of sea ice decline.

Evaluation of model simulations using metrics based on sea ice extent (e.g. Stroeve et al, 2012; Wang and Overland, 2012) is known to be an imperfect method of assessing projections (Notz, 2015). This is partly because of the very high inter-annual variability of sea ice extent (Swart et al, 2015), but also because it does not address the accuracy of the many variables influencing sea ice extent, in which compensating errors may be present. A more fundamental measure of the sea ice state is the sea ice volume, evaluated in CMIP5 by Stroeve et al, 2014 and Shu et al., 2015. However, there remain many variables influencing sea ice volume, and hence this metric is equally susceptible to the problem of compensating errors (although the effect of internal variability on sea ice

https://doi.org/10.5194/gmd-2019-113
Preprint. Discussion started: 19 August 2019

Geoscientific Model Development Discussions

volume is now quite well-understood, e.g. Olonscheck and Notz, 2018). Clearly, a logical next step would be to evaluate the primary driver of sea ice volume, i.e. sea ice mass balance. However, although detailed studies of processes driving Arctic sea ice volume have been undertaken (e.g. Lei et al, 2018), in general these are on too small a scale to directly evaluate model processes.

Many of the processes driving sea ice volume are, to first-order, well understood; sea ice volume is the area integral of sea ice thickness, which is driven by the surface and basal mass budget, and hence energy budget. The surface energy budget is driven partly by variables external to the sea ice, such as fluxes of downwelling shortwave (SW) and longwave (LW) radiation, and air temperature. However it is also influenced by properties of the sea ice state, such as surface temperature, albedo and the top conductive flux. Similarly, the basal energy budget is driven partly by one particular external variable (the ocean heat flux), but also by a property of the sea ice (the basal conductive flux). In turn, these properties of the ice surface and base are determined in the main by ice thermodynamics, which is strongly influenced by ice thickness; the surface albedo is also affected by the ice thickness directly. This closed causal chain (Figure 1) gives rise to the thickness-growth feedback, whereby thinner ice grows more quickly in winter, and the surface albedo feedback, whereby thinner ice melts more quickly in summer.

Sea ice state is determined by the response of the feedback loops to the external variables (downwelling radiation, air temperature, ocean heat flux), which are in turn influenced by the sea ice state over longer timescales. It is difficult to evaluate the simulation of these processes in coupled models due to a lack of large-scale observational datasets. CMIP5 surface radiative fluxes were evaluated by Boeke and Taylor (2018), but the evaluation was unable to separate out flux variability directly caused by sea ice variability. West et al (2019, in discussion) proposed a framework by which external drivers of sea ice mass balance could be separated from feedbacks of the sea ice state given available observations, but the applicability of this framework is limited by observational uncertainty. Hence there remain significant shortcomings in ability to evaluate modelled sea ice processes. In this study, a method is presented of evaluating sea ice mass balance, and sea ice thermodynamics, using data from Arctic ice mass balance buoys, devices that measure ice surface and base elevation and internal ice temperatures.

An observational dataset of sea ice vertical energy fluxes is created by estimating monthly mean fluxes of top melt, top conduction, basal conduction and ocean heat flux for the entire IMB network. The extent to which this dataset is representative of wider regions is investigated by comparing the ice thickness distribution sampled by the buoys to that measured by submarine sonar. Evaluation of the coupled model HadGEM2-ES (part of the CMIP5 ensemble), is then carried out using this dataset. This is done by restricting model data to the densely sampled regions of the North Pole and Beaufort Sea, transforming modelled fluxes to be over ice only, and comparing the distribution of model fluxes obtained for each region and month to that measured from the IMB network. By combining this evaluation with a previous evaluation of the sea ice state and surface radiation in the same model (West et al., 2019, in discussion), a detailed picture of the sea ice simulation emerges, with drivers of model biases easily identifiable.

The study is structured as follows. In section 2, the IMB data, and the process by which vertical energy fluxes are calculated from the data, are described. In section 3, the resulting dataset is presented, and seasonal and spatial

https://doi.org/10.5194/gmd-2019-113
Preprint. Discussion started: 19 August 2019

Geoscientific Model Development Discussions

variability is discussed. In section 4, the data is used to evaluate HadGEM2-ES, and the results are interpreted in the context of West et al (2019). In section 5, the representiveness of the IMB fluxes is discussed. In section 6, conclusions are presented.

2. Calculating monthly-mean energy fluxes from the IMBs

The ice mass balance buoy (IMB; Perovich and Richter-Menge, 2006) is a system of instruments frozen into a sea ice floe, allowing the simultaneous measurement of surface and base elevation, internal ice temperature (usually at 10cm resolution), and position; many also measure surface air pressure and temperature. An IMB provides, by design, measurements of sea ice thickness, and of surface and basal mass balance, via the measurements of surface and base elevation. Fluxes of conduction can also be estimated from the ice temperature data (e.g. Perovich and Elder, 2002), although uncertainty is considerable due to lack of knowledge of ice salinity. In particular, the thermodynamics and basal elevation measurements can be combined to estimate ocean heat flux (Lei et al., 2014).

Data from the 104 IMBs deployed by the Cold Regions Research and Engineering Laboratory (CRREL) are stored in a series of comma-delimited CSV files at http://imb.erdc.dren.mil/buoysum.htm. The buoys were deployed between 1993-2017; spatial coverage is mainly in the North Pole and Beaufort Sea regions (Figure 2). The buoys are identified by the year of deployment followed by a letter, for example '2012L'. All buoys report time series of ice base elevation, snow/ice surface elevation, latitude, longitude, as well as a collection of ice temperature time series taken at a number of vertical positions above, within and below the ice. In general, temperature profiles are reported at very high temporal resolution, hourly or bi-hourly, and tend to be noisy, with much high-frequency variability. From 2006 onwards, elevation data are reported at similarly high resolution, but before 2006 are reported much less frequently, with intervals of a week or more between measurements.

As most analysis of the data depends on the ability to perform arithmetic operations on different series, it was necessary to produce data series at consistent points in time for each buoy. To this end, modified elevation data series were produced at times coincident with the temperature measurements, using either interpolation (where there were fewer than 3 measurements in the 2-day period centred on the time in question) or a binomially-weighted mean (where there were 3 or more measurements in this period). This regularisation process is illustrated in Figure 3.

The set of elevation measurements provided also varies between buoys. The earlier buoys tend to produce data of surface and base elevation only. From these, it is usually possible to deduce snow-ice interface elevation, as by design the snow-ice interface is always at position z=0 at the time of deployment. The process is illustrated in Figure 4: iterating through the times of observation $t_1,...,t_n$, the interface elevation $z_{\text{int}}(t_1)=0m$ by construction. At time t_i, if $z_{\text{int}}(t_{i-1}) \le z_{sfc}(t_i)$, we set $z_{\text{int}}(t_i)=z_{\text{int}}(t_{i-1})$; but if $z_{\text{int}}(t_{i-1}) > z_{sfc}(t_i)$ we set $z_{\text{int}}(t_i)=z_{sfc}(t_i)$. In this way, the interface elevation changes only when top melting of ice is detected, i.e. when the surface elevation is judged to fall below the interface elevation estimated for the previous time of observation.

https://doi.org/10.5194/gmd-2019-113
Preprint. Discussion started: 19 August 2019

Geoscientific Model Development Discussions

This method would fail in the presence of ice flooding and snow-ice formation (e.g. as documented by Provost et al, 2017), but there are no clear signs of such events taking place in any of the IMB records examined in this study. In addition some later buoys do not report surface elevation directly, but report snow-ice interface elevation and snow depth, which must be summed to obtain the surface elevation. Hence full regular time series of surface elevation, snow thickness, interface elevation, ice thickness and base elevation can be obtained for most buoys.

Processing the temperature data is also necessary. Instances of temperature data that are obviously wrong occur very frequently, usually characterised by sudden step changes in the temperature measurements at single, or multiple layers, that are inconsistent with simultaneous measurements in other layers, often to physically unrealistic values. In most cases, wrong values occurred in large groups that were difficult to identify with automatic data processing, and therefore had to be identified by inspection and removed.

For the early buoys, the depths at which temperature measurements are taken are clearly labelled, tending to begin at 60cm or 70cm above the surface, occurring at resolutions of 5cm above the surface and 10cm below. For later buoys, however, the measurement depths are not labelled. It was inferred that for all such buoys, the measurements began at 60cm above the ice surface, descending at a resolution of 10cm. A curious effect occurs with the long-lived buoy 2006C, in which the position of the thermistor string appears to materially change a year after deployment, as the elevation data becomes abruptly dislocated from the temperature contours normally associated with the presence of sea ice and snow. The change occurred soon after the buoy had reported an exceptionally high basal melting flux during the summer of 2007, as reported by Perovich et al (2008). In this case, the instance of the change was estimated, and all temperature data after this point translated downwards by 70cm.

With the processed temperature and elevation data, monthly mean fluxes of top melt, top conduction, basal conduction and ocean heat flux were produced in the following way.

Top melting of ice and/or snow. This flux, commonly reported by models, represents the total energy gain by sea ice (snow) in a grid cell over the course of a month associated with melting of ice (snow) at the upper surface. It is estimated from the IMBs using the surface elevation series. A change between two adjacent daily data points in surface elevation is judged due to top melting if and only if the change is negative. The energy gain associated with the melting is calculated using ice density of 917 kgm^{-2}, snow density of 330kgm^{-2} and latent heat of melting of 3.34 x 10^5 Jkg^{-1}, the standard values used by the sea ice model CICE (Hunke et al, 2013). The daily top melt estimates are then averaged to obtain monthly mean top melt.

Top conductive flux. This flux is defined as the conduction from the snow/ice surface into the ice interior. Its calculation from the IMB data is made difficult by large step changes in temperature gradient associated with the snow-ice interface, which is usually located within 50cm of the upper surface. To calculate top conductive flux, adjusted temperature profiles were calculated for each point in time, in which for each point z above the snow-ice interface, the adjusted temperature can be written as

$$T_{adj} = \mu T + (1-\mu)T_{\text{int}}$$

https://doi.org/10.5194/gmd-2019-113
Preprint. Discussion started: 19 August 2019

Geoscientific Model Development Discussions

where T_{int} is snow-ice interface temperature, and $\mu = k_{ice}/k_{snow}$ where k_{ice} and k_{snow} are ice and snow conductivity respectively; their calculation is described below. A linear fit was then taken through a layer 0-50cm below the snow surface, and multiplied by k_{ice} to produce estimates of instantaneous top conductive flux. These were then averaged to obtain monthly means.

Basal conductive flux. This flux is defined as the conduction from the ice base into the ice interior. As it is a vital component of the energy balance at the ice base it has frequently been estimated from individual buoys in ocean heat flux calculations. Typically, temperature gradients at the ice base are small due to higher salinities here (e.g. Schwarzacher, 1959), with correspondingly higher heat capacities and lower conductivities; hence previous studies have commonly used a reference layer of a fixed thickness above which the basal conduction is estimated. In this study we use the approach of Lei et al. (2014), and calculate the basal conduction by taking temperature gradients across a layer 40cm-70cm above the ice base. As above, the instantaneous values were averaged to a monthly mean.

Ocean heat flux. This flux is defined as the diffusive heat flux arriving at the ice base from the ocean beneath. In theory, it can be calculated as the residual of the basal conductive flux and the latent heat of melting/freezing at the ice base. However, using the basal conductive flux as defined above it is necessary also to take into account the sensible heat uptake of the intervening layer (the 'buffer zone'), 0-40cm above the ice base, illustrated in Figure 5. The ocean heat flux can then be written as

$$F_{ocn} = F_{condbot} - F_{sens} - F_{lat}$$

as in Lei et al (2014).

The basal conductive flux $F_{condbot}$ is defined as above. Monthly mean F_{sens}, the sensible heat flux in the 0-40cm layer, is calculated as the average of daily heat uptake rates obtained by taking linear fits through all temperature points within 1 day of a given time instant for all vertical points in this layer, summing these (weighted according to layer thickness), and multiplying by ice density and heat capacity, defined below. Finally, monthly mean latent heat of melting at the ice base, F_{lat}, is calculated from the base elevation time series, by multiplying daily differences in elevation by specific latent heat of fusion.

The calculation of thermodynamic parameters is now described. Ice conductivity is defined after Maykut and Untersteiner (1971) as

$$k_{ice} = k_{fresh} + \frac{\beta S}{T}$$

where *S* and *T* are ice salinity and temperature respectively, $k_{fresh} = 2.03 Wm^{-1}K^{-1}$, the conductivity of fresh ice, and $\beta = 0.13 Wm^{-1}$ is an empirically determined constant representing the effect of brine pockets on

https://doi.org/10.5194/gmd-2019-113
Preprint. Discussion started: 19 August 2019

conductivity. For the calculation of the top conductive flux, a practical salinity of 1.0 is used, while the temperature used is that of the snow-ice interface. For the calculation of the basal conductive flux, a practical salinity of 4.0 is used, multiplied by the mean value of $1/T$, where the average is taken over the time period in question and the layer 40-70cm above the ice base.

Specific heat capacity is defined after Ono (1967) as

$$c_{ice} = c_{fresh} + \frac{q_{fresh}\mu S}{T^2} \quad (7)$$

where $c_{fresh} = 2106 Jkg^{-1}K^{-1}$ is the specific heat capacity of fresh ice, $q_{fresh} = 3.34\times10^5 Jkg^{-1}$ the specific latent heat of fusion of fresh ice, and $\mu = 0.054K$ the ratio between water salinity and freezing temperature. In calculating sensible heat uptake at the ice base, again a practical salinity of 4.0 is used, multiplied by the mean value of $1/T^2$, where the average is taken over the time period in question and the layer 0-40cm above the ice base.

Ice salinity must also be taken into account when calculating latent heat of freezing and melting. The energy required to melt a given volume of sea ice at temperature *T*, from Bitz and Lipscomb (1999) is

$$q(S,T) = \rho c_0 (T_m - T) + \rho q_{fresh}\left(1 + \frac{\mu S}{T}\right). \quad (8)$$

At the lower surface of the ice, *q* is calculated by setting $T = -1.8°C$ and $S = 4.0$ as above. At the upper surface of the ice, *T* is usually extremely close to 0°C when melting is taking place, meaning that a choice of *S* that is both consistent and physically realistic in all cases is difficult to make. Instead, it is assumed that the ice at the upper surface is fresh, and $q = q_{fresh}$ is used.

The monthly heat fluxes calculated above are subject to two principal sources of uncertainty: measurement uncertainty, and uncertainty in the value of *S*. To estimate the former, we use elevation and temperature measurement uncertainties as described by Perovich and Elder (2002). To estimate the latter, we use an uncertainty of ±1.0 in calculating top conductive fluxes, and an uncertainty of ±4.0 in calculating basal conductive flux, and sensible and latent heat uptake at the ice base. The two uncertainties are added together and combined with the flux central estimates, as defined above, to produce a range of possible monthly mean fluxes for each data point.

Examination of the monthly mean energy fluxes reveals several ways in which unrealistic estimates might be produced. In a small minority of cases, the temperature at the top (bottom) ice surface is inconsistent with the assumption of a salinity range of ±1 (±4), resulting in the observed temperature being above the assumed melting point, and the measured flux being unrealistically large, or in a few cases undefined. Clearly, a more

https://doi.org/10.5194/gmd-2019-113
Preprint. Discussion started: 19 August 2019

Geoscientific Model Development Discussions

comprehensive analysis would allow the selection of varying salinity ranges depending on the information available from each buoy. As this is outside the scope of this study, the fluxes affected by this problem were removed from the dataset.

A second problem relates to the formation of false bottoms under sea ice, as documented by Notz (2003), in which meltwater refreezes upon meeting cold seawater at a temperature below its own melting point. This process visibly occurs during the period of operation of some buoys (for example 2015A, demonstrated in Figure 6), associated with sudden step changes in base elevation. These result in very large negative monthly mean ocean heat fluxes being calculated during the month of formation, and correspondingly large positive fluxes during the month of dissipation. These fluxes are physically unrealistic, as the large changes in elevation usually represent the freezing and melting of only a very thin layer of ice, with liquid seawater remaining in between this layer and the main body of the ice column. Hence it was necessary to inspect each buoy individually for possible false bottom formation, and remove all affected ocean heat fluxes from the dataset.

Unrealistic positive values of top melting occur quite frequently during the winter months, due to decrease of surface elevation likely associated with wind drifting of snow, although these are usually an order of magnitude lower than those observed during the summer months. As a simple way of removing these fluxes, top melt fluxes for all months during which monthly mean surface temperature was measured at -5°C or lower were set to zero. It is noted that during the late spring, this could result in valid top melt fluxes being ignored in the case of rapid rises in temperature during the latter stages of a month.

Unrealistically high negative values of basal conductive flux are also derived during months when the ice was quite thin, and the layer 40cm-70cm above the ice base was correspondingly close to the top surface of the ice. In order to account for this situation, basal conductive fluxes (and oceanic heat fluxes) for all months during which monthly mean ice thickness was 1m or lower were removed from the dataset.

3. Deriving monthly-mean flux distributions from the IMBs

Throughout the description of the IMB-estimated fluxes here, and the model evaluation below, the convention used is that positive numbers denote downwards fluxes, and vice versa. The distributions of monthly mean fluxes of top melting, top conduction, basal conduction and ocean heat flux are summarised in Table 1. The IMBs provide 490 monthly mean values of top melt in total, ranging from 31 values in March and August to 57 in May. The seasonal cycle reaches its maximum in July, when top melting of 28.6 ± 16.7 Wm^{-2} is observed. Strong top melting is also evident in June (16.1 ± 10.1 Wm^{-2}), but top melting tends to be considerably lower in August (7.8 ± 6.4 Wm^{-2}). Values for the rest of the year are zero or near-zero. Throughout the year, standard deviation of the distributions is of a similar order of magnitude to the mean, showing a high degree of spatial and inter-annual variability.

Top conductive flux, a component of the surface energy balance, is the means by which the ice loses energy to the atmosphere in the presence of atmospheric cooling during the Arctic winter. It depends strongly upon

https://doi.org/10.5194/gmd-2019-113
Preprint. Discussion started: 19 August 2019

Geoscientific Model Development Discussions

atmospheric conditions, but also upon ice and snow thickness, as thinner ice and snow can support stronger temperature gradients and conduct energy upwards more quickly. For the top conductive fluxes, the IMBs provide 501 estimates in total, ranging from 30 in August to 59 in May. Mean top conductive fluxes are strongly negative from October-March, reaching a minimum value of -22.3 ± 13.2 Wm^{-2} in December. However, values are weakly positive in June and July, reflecting warming of the ice interior.

The basal conductive flux acts to remove energy from the ice base in winter, allowing ice growth, and to a lesser extent during late spring and early summer while the ice is warming, attenuating ice melt. For the basal conductive fluxes the IMBs provide 473 estimates, ranging from 27 in August to 54 in May. The basal conductive flux displays a seasonal cycle less amplified than, and displaced slightly later relative to, that of the top conductive flux, with lowest values occurring from November-April and a minimum of -13.6 ± 6.4 Wm^{-2} occurring in February. The damped response relative to the top conductive flux occurs due to the thermal inertia of sea ice, and the principal thermodynamic forcing occurring at the top surface.

Lastly, for the ocean heat fluxes the IMBs provide 436 estimates, ranging from 26 in August to 48 in May. The highest values are seen in August, with a mean and spread of 25.1 ± 28.7 Wm^{-2}. The distribution is also strongly positively skewed in this month, with a small number of exceptionally high values, notably 143 Wm^{-2} being estimated in August 2007 for buoy 2006C in the Beaufort Sea, as part of a summer of extreme ice melt documented by Perovich et al. (2008). In the winter, mean values of ocean heat flux are near-zero. There is frequent occurrence of small negative estimates in the distributions in the winter. These are likely to be spurious and reflect errors in assumptions made about the salinity and density at the base of the ice, as for most such values, the uncertainty intervals encompass 0 Wm^{-2}.

Two regions of the Arctic are relatively densely sampled by the IMBs: the Beaufort Sea and the North Pole (Figure 2). In order to demonstrate that the IMBs are able to capture some regional variability, and especially to aid with model evaluation in Section 4 below, monthly mean fluxes derived from buoy tracks entirely within these regions were sorted into separate datasets, characteristics of which are now described separately.

Top melting fluxes are shown in Figure 7a separately for the Beaufort Sea and the North Pole regions. In June, the top melting fluxes measured in the North Pole region range from 1-32 Wm^{-2}, with a mean of 11 ± 7 Wm^{-2}, while those measured in the Beaufort Sea range from 4-48 Wm^{-2} with a mean of 22 ± 11 Wm^{-2}. The lower distribution in the North Pole region is consistent with the observed later onset of surface melting here (Markus et al., 2009) associated with the higher latitude. In July, measured fluxes range from 2-48 Wm^{-2} in the North Pole region, with a mean of 22 ± 12 Wm^{-2}, and 11-70 Wm^{-2} in the Beaufort Sea region, with a mean of 40 ± 16 Wm^{-2}. Measured fluxes of top melting are much lower in August in both regions.

For the top conductive flux (Figure 7b), winter variability is somewhat higher over the Beaufort Sea region than in the North Pole region. In December, North Pole fluxes range from -45 to -9 Wm^{-2} with a mean of -20 ± 10 Wm^{-2}, while those in the Beaufort Sea region range from -57 to -8 Wm^{-2} with a mean of -28 ± 14 Wm^{-2}. Some notable differences between the distributions occur in the 'shoulder seasons', particularly in May and September, with higher values (indicating ice warming) occurring in the Beaufort Sea region. For example, in May, values in the

https://doi.org/10.5194/gmd-2019-113
Preprint. Discussion started: 19 August 2019

Geoscientific Model Development Discussions

North Pole region range from -8 to 5 Wm^{-2} with a mean of -2 ± 3 Wm^{-2}, while values in the Beaufort Sea region range from -2 to 15 Wm^{-2} with a mean of 2 ± 4 Wm^{-2}. These differences indicate earlier onset of warming in the Beaufort Sea and earlier onset of cooling in the North Pole region, consistent with an earlier onset of surface melt in the Beaufort Sea.

Less spatial variability is evident for the basal conductive flux (Figure 7c). For example, in December, North Pole fluxes range from -20 to 0 Wm^{-2} with a mean of -12 ± 5 Wm^{-2}, while Beaufort Sea fluxes range from -22 to -2 Wm^{-2} with a mean of -12 ± 6 Wm^{-2}. Hence the thermal inertia of ice appears to have some damping effect on the larger variability of thermal forcing evident in the Beaufort Sea region from the top conductive flux. The faster warming and slower cooling of ice evident in the shoulder seasons in the Beaufort Sea region for the top conductive flux is also not evident for the basal conductive flux. In the month of May, for example, basal conductive flux values range from -13 to 0 Wm^{-2} in the North Pole region with a mean of -7 ± 3 Wm^{-2}, compared to a range of -8 to -3 Wm^{-2} and a mean of -5 ± 1 Wm^{-2} in the Beaufort Sea region.

For the ocean heat flux (Figure 7d), in the summer very high values tend to be more common in the Beaufort Sea region than in the North Pole region. For example, in August North Pole region values range from 3 to 64 Wm^{-2} with a mean of 19 ± 16 Wm^{-2}, while the Beaufort Sea region values range from 7 - 143 Wm^{-2} with a mean of 41 ± 48 Wm^{-2}. It is likely that these are related to the lower ice fractions, and greater solar heating of the mixed layer, in the Beaufort Sea region.

4. Evaluating modelled sea ice using the IMB-derived fluxes

4.1 Evaluating vertical energy fluxes in HadGEM2-ES with the IMBs

In this section, the distributions of energy fluxes estimated from the IMB data are compared to equivalent fluxes simulated by the coupled climate model HadGEM2-ES. This model, developed from the earlier model HadGEM1, is based on the HadGEM2-AO coupled atmosphere-ocean system, but employs additional components to simulate terrestrial and oceanic ecosystems, and tropospheric chemistry (Collins et al., 2011). The sea ice component is very similar to that used by HadGEM1 (McLaren et al., 2006), employing a sub-gridscale thickness distribution with 5 categories (Thorndike et al., 1975), elastic-viscous-plastic rheology (Hunke and Dukowicz, 1997), and a zero-layer thermodynamics scheme, described in the appendix to Semtner (1979), in which sea ice has no heat capacity and conduction does not vary with height within the ice. The atmosphere and ocean components contain a number of improvements relative to HadGEM1 (Martin et al., 2011).

The Arctic sea ice and surface radiation simulation of the historical ensemble of HadGEM2-ES was evaluated by West et al (2018). A number of likely model biases were identified; a low bias in September sea ice extent, a low bias in annual mean ice thickness and a high bias in ice thickness seasonal cycle amplitude, and a tendancy to model overly high surface net downwelling shortwave (SW) flux in summer and overly low surface net downwelling longwave (LW) flux in winter. To perform the evaluation of the ice energy budget in the present study, the model period 1980-1999 is used, chosen to match the period used in West et al (2018).

https://doi.org/10.5194/gmd-2019-113
Preprint. Discussion started: 19 August 2019

Geoscientific Model Development Discussions

For each month, grid cells lying inside the North Pole and Beaufort Sea regions are separately identified, and monthly mean top melt flux, top conductive flux, basal conductive flux and ocean heat flux are collected into distributions. Means and standard deviations of these distributions are then compared to those of the IMB fluxes, with model fluxes weighted by grid cell area when calculating these statistics. Before aggregation the fluxes, produced by the model as gridbox means, are divided by ice area to produce means over ice only, for greater consistency with the IMB fluxes. Owing to the zero-layer thermodynamics scheme, sea ice conduction is constant with depth, and hence top and basal conductive fluxes are always equal in the model.

For both regions, top melt fluxes simulated by HadGEM2-ES tend to be much higher than those measured by the IMBs (Figure 8a,b). For example, the modelled mean top melt flux of 72.5 ± 8.2 Wm^{-2} in the Beaufort Sea region in June is much higher than the IMB mean of 24.5 ± 9.4 Wm^{-2}; in the North Pole region in June, the modelled mean top melt flux of 56.6 ± 14.0 Wm^{-2} is much higher than the IMB mean of 11.2 ± 6.9 Wm^{-2}. The phase of the annual cycle in top melt is shifted slightly earlier, with the effect that, in both regions, the modelled June and July means are very similar while the IMB estimates show a distinct maximum in July. However, the greater top melt in the Beaufort Sea region relative to the North Pole region is captured by the model.

The annual cycle of top conductive flux is broadly captured by HadGEM2-ES (Figure 8c,d), with strongly negative values modelled in the autumn, winter and spring and weakly positive values in the summer. However, from September-May modelled means are more strongly negative than observed means: for example, in the North Pole region in December a modelled mean of -31.0 ± 7.6 Wm^{-2} is higher in magnitude than the IMB mean of -20.4 ± 10.3 Wm^{-2}. The higher magnitude of conductive fluxes in winter in the Beaufort Sea region relative to the North Pole region is captured by the model; however, the higher values of fluxes in May and September in the Beaufort Sea region relative to the North Pole region are not captured.

Modelled values of basal conductive flux at each model gridbox, as noted above, are identical to those of top conductive flux. Consequently HadGEM2-ES overestimates the magnitude of basal conductive flux in autumn and winter more severely than it does top conductive flux (Figure 8e,f). The overestimation is most severe during the autumn; in the Beaufort Sea region in October a mean modelled flux of -28.1 ± 11.1 Wm^{-2} is much higher in magnitude than the mean observed flux of -3.2 ± 5.2 Wm^{-2}. As the basal conductive flux in the freezing season is the principal driver of ice growth, this suggests that HadGEM2-ES is likely to model significantly stronger ice growth during these months than was measured at the IMB sites.

For the ocean heat flux, the model produces a similar seasonal cycle to that estimated from the IMB data, with very small values in the winter and a wide range of positive values in the summer. For the North Pole region, the distribution means are very similar in August but the observed spread far wider, with a modelled mean of 23.5 ± 10.0 Wm^{-2} comparing to an observed mean of 18.8 ± 16.0 Wm^{-2}; however, modelled values are larger than observed earlier in the summer, with evidence of a phase offset between model and observations. The larger spread in the IMB estimates is consistent with a comparison of observed point values to modelled means over grid cells. For the Beaufort Sea region, the modelled mean of 26.6 ± 12.0 Wm^{-2} is much lower than the IMB-estimated value of 42.4 ± 44.1 Wm^{-2}. It is possible that the discrepancy here is caused by the observed rapid retreat of summer sea ice in the Beaufort Sea in the past 15 years, with accompanying direct solar heating of the ocean mixed layer, and

https://doi.org/10.5194/gmd-2019-113
Preprint. Discussion started: 19 August 2019

Geoscientific Model Development Discussions

the increased occurrence of exceptionally high values of ocean heat flux. These effects are not represented in the HadGEM2-ES simulation in the 1980-1999 period.

4.2 Links to sea ice and surface radiation simulation of HadGEM2-ES

A top melting bias of ~40 Wm^{-2} is estimated for the month of June in both the North Pole and Beaufort Sea regions. This is consistent with the finding of West et al (2018) that June surface net shortwave (SW) radiation in the model was biased high relative to a variety of satellite and reanalysis datasets, by around 20 Wm^{-2} over the Arctic Ocean on average. Relative to CERES-EBAF measurements from 2000-2013 (Loeb et al., 2009), HadGEM2-ES overestimates June net SW in the North Pole and Beaufort Sea regions by 30 and 9 Wm^{-2} respectively. Owing to the recent trend to earlier onset of surface melt over the past 30 years (e.g. Markus et al., 2009), and attendant likely decrease in surface albedo, these biases are likely to be underestimated. Hence it is likely that a major part of the model bias in top melting can be explained by a model bias in net SW. In West et al (2018) it was shown that a tendency for surface melt onset to occur too early in HadGEM2-ES, reducing the surface albedo, was likely to be principally responsible for this.

The severe overestimation in magnitude of basal conductive fluxes during the early part of the melt season can be partly explained by the zero-layer thermodynamics scheme of HadGEM2-ES; the thermal inertia effect seen in the IMBs, whereby the basal conductive flux drops much more slowly in autumn than the top conductive flux, does not occur in the model. However, as the top conductive fluxes also tend to be considerably higher in the model than in the IMB estimates, the thermal inertia effect is likely to be only partially responsible. In West et al (2018) two other model biases were identified as being likely to lead to a high bias in winter ice growth (analogous to the basal conductive flux bias): a negative bias in ice thickness during early winter, and a negative bias in downwelling longwave (LW) radiation throughout the season. It was estimated that these biases were likely to lead to surface flux biases of order ~10 Wm^{-2} throughout the freezing season. Hence these are also likely to explain a portion of the basal conductive flux bias noted above.

The excessive modelled top melting and basal conductive fluxes identified would be likely to lead to too strong ice growth, and ice melting, in winter and summer respectively, and an associated amplification of the ice thickness seasonal cycle. Such an amplification was identified in HadGEM2-ES by comparing modelled ice thickness to the forced ice-ocean model PIOMAS, as well as to estimates from satellites and submarines. Hence there is a high level of consistency between the model biases inferred from the IMB estimates, and those inferred from the sea ice state and surface radiation evaluations in West et al (2018). The IMB evaluation, however, provides additional insight to the picture, by providing consistent evaluation of previously unknown processes such as top melting. In addition the IMB evaluation clearly identifies a role for the zero-layer thermodynamics scheme in driving a bias towards excess ice growth during the early winter in HadGEM2-ES.

5. Representativeness of the IMB-estimated fluxes

https://doi.org/10.5194/gmd-2019-113
Preprint. Discussion started: 19 August 2019

Geoscientific Model Development Discussions

The comparison of HadGEM2-ES modelled fluxes to those inferred from the IMB measurements reveals several potential model biases, notably the overestimation of top melt flux in June and July, and overestimation of the magnitude of basal conductive flux in the early freezing season. In this section the accuracy of this method of model bias estimation is discussed.

The model flux distributions evaluated represent area-weighted means over the ice-covered fractions of grid cells, each of order 10-100 km in width, chosen to cover the North Pole and Beaufort Sea regions as defined in Section 2. The 'true model bias' would represent the difference between this and the average flux over ice covered regions for each month in the 1980-1999 period. By contrast, the IMB-measured means are derived from a relatively small number of single point measurements from these regions (points that tend to move position during an individual month, with the general ice flow), most from a period somewhat later than 1980-1999. To assess the accuracy of the model biases inferred, a method of estimating the order of magnitude of the likely error in the IMB estimated mean fluxes is required.

One source of error derives from the temporal offset in the IMB measurements relative to the model. To assess the impact of this, we compare the HadGEM2-ES vertical ice fluxes from the period 1980-1999 to those from the period 2000-2015, during which most of the IMB measurements were taken (as the historical experiments end in 2005, the RCP8.5 experiment was used from 2006 onwards). Flux anomalies in the later period relative to the earlier period are mostly small (below 2 Wm^{-2} in magnitude) in both regions. However, there is a significant negative anomaly in July top melting, -6 Wm^{-2} and -9 Wm^{-2} in the North Pole and Beaufort Sea regions respectively. There is also a positive anomaly in September basal conductive flux (3 Wm^{-2} in both regions), and in the Beaufort Sea moderate basal conductive flux anomalies continue into the winter, being 5, 3, -4 and -2 Wm^{-2} from October-January respectively. These anomalies are likely to reflect earlier melting and later freezing of ice in this region. They are small in size compared to the HadGEM2-ES model biases, but suggest that the temporal bias may cause model top melting bias in July, and Beaufort Sea basal conductive flux in autumn, to be slightly overstated.

A potentially more serious source of error is sampling: bias would be introduced if the IMB measurements were systematically over- or under-sampling locations with higher than average flux in a particular month. The Arctic sea ice cover is highly heterogeneous, with ice conditions varying substantially over all scales. For most variables (for example snow thickness, ice salinity or ice albedo), it is difficult to assess whether the variability of the ice pack is sufficiently sampled by the IMB measurements, due either to a lack of reference datasets or to an inability to estimate these variables at the IMB locations. However, the degree to which the ice thickness distribution (which affects conductive fluxes in particular) is correctly sampled by the IMBs can be assessed. The effect of errors in the ice thickness distribution on the IMB-measured fluxes is estimated in Appendix A, and is shown to be small compared to the model biases identified. We note that the ice thickness distribution sampling bias is likely to be particularly strong (relative to other variables) due to the deliberate placing of IMBs in level multiyear ice, and due to the Lagrangian movement of the IMBs combined with the generally short lifetime of thin ice floes, which tend to grow quickly in winter and melt quickly in summer. It is proposed that given the effect of this bias is weak, it is likely that the effect of other, not deliberately introduced, biases is weaker still, and that the model biases identified in Section 4 are likely to be robust features.

https://doi.org/10.5194/gmd-2019-113
Preprint. Discussion started: 19 August 2019

Geoscientific Model Development Discussions

6. Conclusions

Around 500 estimates of monthly mean top melt, top conduction, basal conduction and ocean heat flux have been estimated from data measured by the Arctic IMB network, with the number of estimates available for each month ranging from 26 to 59. The distributions capture seasonal and spatial variation in the vertical fluxes analysed, and provide a valuable source of information on the internal energy balance of Arctic sea ice. Comparison of modelled fluxes to observed fluxes in the two densely sampled regions in the North Pole and Beaufort Sea reveals substantial model biases, notably to high top melt fluxes in summer and to high (negative) basal conductive fluxes in autumn and early winter. Biases in the IMB flux estimates due to inadequate sampling of thin and very thick ice types are likely to be small relative to the model biases identified.

The flux biases are consistent with an evaluation of the sea ice simulation of HadGEM2-ES that identified an over-amplified seasonal cycle in ice thickness, with model ice growth and melt biased high in winter and summer respectively, as well as a high model bias in net SW radiation in June, a low bias in net LW radiation throughout the winter, and a low model bias in ice thickness in autumn and early winter. The IMB analysis confirms that the net SW bias is likely to cause overly strong ice thinning during summer via anomalously strong top melting of ice, and that the cold atmospheric conditions and low ice thickness of HadGEM2-ES are likely to be driving anomalously strong winter ice growth via the basal conductive flux. However, the IMB analysis also suggests that the zero-layer thermodynamic scheme of HadGEM2-ES plays a role in promoting this anomalously strong ice growth.

The calculated IMB fluxes offer a potentially valuable tool for increasing understanding of sea ice simulations in coupled models, as they allow detailed examination of the links between atmospheric forcing of sea ice and the resulting sea ice state. This is particularly the case for the upcoming Phase 6 of the Coupled Model Intercomparison Project (CMIP6), for which diagnostics of ice energy and mass fluxes, such as top melting and conduction, have been requested for all sea ice models participating in this experiment (Notz et al., 2016). Understanding of the processes leading to biases in a given sea ice state enables better understanding of modelled sea ice spread in the present day and in the future, and may therefore also allow better understanding of future projections in sea ice state.

By far the greatest source of uncertainty in estimating the IMB fluxes derives from lack of knowledge of ice salinity at the measurement sites, and therefore the thermodynamic properties of conductivity and heat capacity. A method of measuring salinity at the IMB sites would greatly reduce the uncertainty in the IMB estimates, particularly for ocean heat flux, enhancing the usefulness of this dataset as a tool for model evaluation.

Appendix A: The ice thickness sampling bias and its effect on flux distributions

https://doi.org/10.5194/gmd-2019-113
Preprint. Discussion started: 19 August 2019

Geoscientific Model Development Discussions

An analysis of the distribution of monthly mean ice thicknesses sampled by the IMBs finds that most lie in the range 1.4 – 3.6 m. However, analysis of submarine measurements of ice thickness in the Central and Western Arctic from 1981-2000, as collated by Rothrock et al. (2008), shows a substantial proportion of ice to be of thickness outside these bounds. In order to estimate the effect of this sampling bias, we use the following simple model. The thickness distribution is discretised, in a similar manner to HadGEM2-ES, by separating ice into five thickness categories, with minimum thickness bounds at 0 m, 0.6 m, 1.4 m, 2.4 m and 3.6 m. Given a mean flux $F_{IMB}^{m,r}$ for month *m* and region *r* that is estimated from the IMBs by averaging all fluxes for that month and region, the total observational error can be characterised as

$$F_{err} = F_{IMB}^{m,r} - F_{actual}^{m,r} \qquad \text{(A1)}$$

where $F_{actual}^{m,r}$ is the actual value of that flux, averaged over the region and month in question, for the period 1993-2015. The mean flux can be further split into thickness categories by setting

$$F_{IMB}^{m,r} = \sum_i F_{IMB-cat}^{m,r,i} \bullet \left(N_i^{m,r} / N_{total}^{m,r} \right) \qquad \text{(A3)}$$

where the $F_{IMB-cat}^{m,r,i}$ are the average IMB flux over month *m*, region *r* and category *i*, $N_i^{m,r}$ is the total number of IMB fluxes in month *m*, region *r* and category *i,* and $N_{total}^{m,r}$ is the total number of IMB fluxes in month *m* and region *r*.

Similarly the actual flux values can be written as

$$F_{actual}^{m,r} = \sum_i F_{actual-cat}^{m,r,i} \bullet a_i^{m,r} \qquad \text{(A4)}$$

where $a_i^{m,r}$ is the average fraction of ice in month *m* and region *r* that is in category *i* (expressed as a proportion of average fraction of ice in the region).

It can be seen that $N_i^{m,r} / N_{total}^{m,r}$ acts as an IMB-based estimate of $a_i^{m,r}$, and that the error in $F_{IMB}^{m,r}$ due to the ice thickness sampling bias is exactly that due to the error in this estimate. Hence we can characterise the sampling error by expressing F_{err} in terms of systematic and sampling errors in the following way:

https://doi.org/10.5194/gmd-2019-113
Preprint. Discussion started: 19 August 2019

Geoscientific Model Development Discussions

$$
\begin{aligned}
F_{err}^{m,r} &= \sum_i \left(F_{IMB-cat}^{m,r,i} \bullet \left(N_i^{m,r} / N_{total}^{m,r} \right) - F_{actual-cat}^{m,r,i} \bullet a_i^{m,r} \right) \\
&= F_{err\_systematic} + F_{err\_sample} \\
&= \frac{1}{2} \sum_i \left(F_{IMB-cat}^{m,r,i} - F_{actual-cat}^{m,r,i} \right) \left(N_i^{m,r} / N_{total}^{m,r} + a_i^{m,r} \right) \\
&\quad + \frac{1}{2} \sum_i \left(N_i^{m,r} / N_{total}^{m,r} - a_i^{m,r} \right) \left(F_{IMB-cat}^{m,r,i} + F_{actual-cat}^{m,r,i} \right)
\end{aligned}
\qquad \text{(A5)}
$$

where F_{err_sample} captures the flux error due to ice thickness sampling; $F_{err\_systematic}$ describes the error due to inaccuracy in the IMBs estimating F for each particular category, effectively capturing the remaining observational error that is beyond the scope of the current analysis.

To estimate F_{err_sample}, we first need estimates of $a_i^{m,r}$, the real-world proportion of ice in a given thickness category for each region and month, for which as discussed above we use submarine measurements collated by Rothrock (2008) that capture small-scale variation in sea ice thickness. Ice thickness measurements in each category are collected for each month and region, and used to generate an estimate of $a_i^{m,r}$. In practice, measurements are abundant during spring and autumn, but sparse during summer and non-existent during winter. To alleviate this problem, we interpolate $a_i^{m,r}$ using a 5-month binomial mean, weighted by number of measurements, in order to produce a smooth seasonal cycle, motivated by the observation that maximum and minimum ice thickness values often occur during spring and autumn respectively. The resulting seasonal cycles of $a_i^{m,r}$ are shown in Figure A1.

Secondly, estimates of $\frac{1}{2}\left(F_{IMB-cat}^{m,r,i} + F_{actual-cat}^{m,r,i}\right)$, representative average fluxes for each thickness category, are required. To calculate representative fluxes of conduction, we combine a simple model of the relationship between conductive fluxes and ice and snow thickness with the IMB measurements of conduction. The surface flux $F_{sfc} = F_{atmos} + BT_{sfc}$ is approximated by linearising the dependence on surface temperature T_{sfc}, referenced to 0°C. The surface flux is set equal to the top conductive flux $F_{condtop}$, and a constant rate of change of conductive flux from the top to the basal surface of the ice is assumed, such that $\frac{1}{2}\left(F_{condtop} + F_{condbot}\right) = \frac{\left(T_{sfc} - T_{bot}\right)}{R_{ice}}$, where $F_{condbot}$ represents basal conductive flux, T_{bot} ice base temperature, and $R_{ice} = h_{ice}/k_{ice} + h_{snow}/k_{snow}$ is the thermal insulance of the ice-snow column, h_{ice} and h_{snow} being ice and snow thickness, and k_{ice} and k_{snow} ice and snow conductivity respectively. Eliminating T_{sfc} from the above equations gives

$$
F_{condtop} = \frac{F_{atmos} + BT_{bot}}{1 - BR_{ice}^{HS-top}} \qquad \text{(A6)}
$$

https://doi.org/10.5194/gmd-2019-113
Preprint. Discussion started: 19 August 2019

Geoscientific Model Development Discussions

where $R_{ice}^{HS-top} = R_{ice} / (1 + \alpha_{heat})$ and $\alpha_{heat} = \frac{F_{condtop} - F_{condbot}}{F_{condtop} + F_{condbot}}$.

Equation (A6) can be combined with the IMB estimates of conductive fluxes, and snow and ice thickness to produce, for each monthly mean IMB measurement, an associated value of F_{atmos}, a measure of the atmospheric forcing on the ice that is independent of small-scale variations in ice thickness. Hence for each month and region a distribution in F_{atmos} can be produced; mean values of this can be fed back into the simple model to produce an average conductive flux that would be expected for each ice thickness category. The average conductive flux is then multiplied by $\left(N_i^{m,r} / N_{total}^{m,r}\right) - a_i^{m,r}$, as estimated above, and summed over categories to produce the flux error $F_{err}^{m,r}$.

The resulting flux bias is below 1 Wm^{-2} in magnitude year-round in the North Pole region. It is slightly larger in the Beaufort Sea in winter time, achieving values of -1.5 Wm^{-2} to -1 Wm^{-2} from November-February. The values are small compared to the model-observation differences identified in Section 4, and so we conclude that the ice thickness sampling bias does not seriously affect ability to evaluate modelled conductive fluxes.

A less strong, but still discernible, relationship exists between top melt flux and ice thickness, due to ice albedo tending to be lower for thinner ice. However, this effect is likely to be associated with a significant difference in albedo only for the thinnest category of ice, and then only in the absence of snow (e.g. Ebert et al., 1995). To estimate this effect, we use an average albedo of 0.55 for bare ice in the top four thickness categories, and 0.35 in the lowest category, based on observed values reviewed and collated by Pirazzini (2008). We assume that ice is snow-covered 80% of the time from October-May (with a corresponding albedo of 0.85), 50% of the time in June and September, and 20% of the time in July and August. Finally, we calculate mean values of downwelling SW radiation for the North Pole and Beaufort Sea region from CERES-EBAF from 2000-2013, and multiply these by the albedo differences implied by the anomaly of ice fraction in category 1. With this method, a maximum flux bias of -3 Wm^{-2} is estimated for the North Pole region, in July, and of -2 Wm^{-2} for the Beaufort Sea region, also in July. Again, this anomaly is small compared to the model-observation differences seen in Section 4, and it is concluded that the sampling bias similarly does not affect ability to evaluate modelled top melting.

An estimate of the influence of the sampling bias on ocean heat flux estimates is more difficult, due to a less clear relationship between ice thickness and the ocean heat flux, and the frequent presence of rapid changes in ice thickness during the months in which ocean heat flux is highest (July and August). It is likely that very small ice thicknesses are associated with elevated ocean heat flux in the summer months due to greater solar penetration through ice. However, the ice thickness sampling bias is at its least severe during the summer months, as thinner ice is sampled by the IMBs simply through the melting of originally thicker floes on which the IMBs were placed. In addition, thinning ice which induces a particularly high ocean heat flux is likely to melt out quickly, and contribute a correspondingly small fraction to the ice thickness distribution.

https://doi.org/10.5194/gmd-2019-113
Preprint. Discussion started: 19 August 2019

Geoscientific Model Development Discussions

We examined the sensitivity of the average ocean heat fluxes to this issue by assuming ocean heat fluxes in category 1 to be systematically larger than those in the remaining categories (as diagnosed from the IMBs) by a factor λ. With λ=3, August ocean heat fluxes in the Beaufort Sea region are on average 80Wm-2 greater in category 1 than in thicker ice categories; it is unlikely that the solar penetration effect could be associated with larger flux differences than this. The largest average flux bias associated with this effect is then -6.3 Wm-2, also seen in August in the Beaufort Sea region. Hence this could be taken as a reasonable upper bound for the effect of the sampling bias on ocean heat fluxes. It is smaller in magnitude than the model ocean heat flux biases diagnosed, although the difference is less than those for the top melt and conductive fluxes.

Code availability

The copyright to the code used in this study is owned by the Met Office. A licence allowing access and use of the code by the general public for research purposes is not yet available. Hence it is not possible to publish the code with this article. Code may be requested from the authors by email.

Data availability

The IMB data is publicly available, and can be downloaded from http://imb.erdc.dren.mil/buoysum.htm. However, the diagnostics from HadGEM2-ES used in this study are not publicly available.

Acknowledgements

This work was supported by the Joint UK BEIS/Defra Met Office Hadley Centre Climate Programme (GA01 101), and the European Union's Horizon 2020 Research & Innovation programme through grant agreement No. 727862 APPLICATE. MC was supported by NE/N018486/1.

Author contribution

The IMB-derived fluxes were calculated, and the subsequent model evaluation performed, by Alex West. The analysis of sampling error in the Appendix was designed and carried out by Alex West. The paper was written in its final form by Alex West with assistance from Mat Collins and Ed Blockley.

References

Bitz, C. and Lipscomb, W. H.: An energy-conserving thermodynamic model of sea ice, J. Geophys. Res. (Oceans), 104, C7, 15669-15677. doi: 10.1029/1999JC900100, 1999

Boeke, R. C. and Taylor, P. C.: Evaluation of the Arctic surface radiation budget in CMIP5 models. J. Geophys. Res. (Atmos), 121, 14, 8525-8548. doi: 10.1002/2016JD025099, 2016.

https://doi.org/10.5194/gmd-2019-113
Preprint. Discussion started: 19 August 2019

Collins, W. J., Bellouin, N., Doutriaux-Boucher, M., Gedney, N., Halloran, P., Hinton, T., Hughes, J., Jones, D., Joshi, M., Liddicoat, S., Martin, G., O'Connor, F., Rae, J., Senior, C., Sitch, S., Totterdell, I., Wiltshire, A. and Woodward, S.: Development and evaluation of an Earth-System model – HadGEM2. Geosci. Model Dev., 4, 1051-1075. doi:10.5194/gmd-4-1051-2011, 2011

Ebert, E. E., Schramm, J. L. and Curry, J. C.: Disposition of solar radiation in sea ice and the upper ocean, J. Geophys. Res., 100, C8, 15,965-15,975. doi: 10.1029/95JC01672

Hunke, E. C. and Dukowicz, J. K., An Elastic–Viscous–Plastic Model for Sea Ice Dynamics, J. Phys. Oceanogr., 27, 9, 1849–1867, doi: https://doi.org/10.1175/1520-0485(1997)027<1849:AEVPMF>2.0.CO;2, 1997.

Lei, R., Li, N., Heil, P., Cheng, B., Zhang, Z. and Sun, B.: Multiyear sea ice thermal regimes and oceanic heat flux derived from an ice mass balance buoy in the Arctic Ocean, J. Geophys Res (Oceans), 119, 1, 537-547. doi: 10.1002/2012JC008731, 2014

Lei, R., Cheng, B., Heil, P., Vihma, T., Wang, J., Ji, Q and Zhang, Z.: Seasonal and Interannual Variations of Sea Ice Mass Balance From the Central Arctic to the Greenland Sea. J. Geophys. Res. (Oceans), 123, 4, doi: 10.1002/2017JC013548, 2018.

Lindsay, R. and Schweiger, A.: Arctic sea ice thickness loss determined using subsurface, aircraft, and satellite observations. The Cryosphere, 9, 269-283. doi: 10.5194/tc-9-269-2015, 2015

Loeb, N. G., Wielicki, B. A., Doelling, D. R., Louis Smith, G., Keyes, D. F., Kato, S., Manalo-Smith, N. and Wong, T.: Toward Optimal Closure of the Earth's Top-of-Atmosphere Radiation Budget. J Cli, 22, 3, 748–766. doi: 10.1175/2008JCLI2637.1, 2009

Markus, T., Stroeve, J. C. and Miller, J.: Recent changes in Arctic sea ice melt onset, freezeup, and melt season length, J. Geophys. Res. (Oceans), 114, C12. doi: 10.1029/2009JC005436, 2009

Martin, G. M., Bellouin, N., Collins, W. J., Culverwell, I. D., Halloran, P. R., Hardiman, S. C., Hinton, T. J., Jones, C. D., McDonald, R. E., McLaren, A. J., O'Connor, F. M., Roberts, M. J., Rodriguez, J. M., Woodward, S., Best, M. J., Brooks, M. E., Brown, A. R., Butchart, N., Dearden, C., Derbyshire, S. H., Dharssi, I., Doutriaux-Boucher, M., Edwards, J. M., Falloon, P. D., Gedney, N., Gray, L. J., Hewitt, H. T., Hobson, M., Huddleston, M. R., Hughes, J., Ineson, S., Ingram, W. J., James, P. M., Johns, T. C., Johnson, C. E., Jones, A., Jones, C. P., Joshi, M. M., Keen, A. B., Liddicoat, S., Lock, A. P., Maidens, A. V., Manners, J. C., Milton, S. F., Rae, J. G. L., Ridley, J. K., Sellar, A., Senior, C. A., Totterdell, I. J., Verhoef, A., Vidale, P. L. and Wiltshire, A., The HadGEM2 family of Met Office Unified Model climate configurations, Geosci. Model Dev., 4, 723-757, doi: https://doi.org/10.5194/gmd-4-723-2011, 2011

https://doi.org/10.5194/gmd-2019-113
Preprint. Discussion started: 19 August 2019

Massonnet, F., Fichefet, T., Goosse, H., Bitz, C. M., Philippon-Berthier, G., Holland, M. M. and Barriatt, P.-Y., Constraining projections of summer Arctic sea ice, The Cryosphere, 6, 1383–1394, doi: 10.5194/tc-6-1383-2012, 2012.

Maykut, G. A. and Untersteiner, N.: Some results from a time-dependent thermodynamic model of sea ice, J. Geophys Res (Oceans and Atmospheres), 76, 6, 1550-1575. doi: 10.1029/JC076i006p01550, 1971.

McLaren, A. J., Banks, H. T., Durman, C. F., Gregory, J. M., Johns, T. C., Keen, A. B., Ridley, J. K., Roberts, M. J., Lipscomb, W. H., Connolley, W. M. and Laxon, S. W.: Evaluation of the sea ice simulation in a new coupled atmosphere-ocean climate model (HadGEM1). J. Geophys. Res., 111, C12014. doi: 10.1029/2005JC003033, 2006.

Notz, D., McPhee, M. G., Worster, M. G., Maykut, G. A., Schlunzen, K. H. and Eicken, H.: Impact of underwater-ice evolution on Arctic summer sea ice, J. Geophys. Res. (Oceans), 108, C7, doi: 10.1029/2001JC001173, 2003

Notz, D.: How well must climate models agree with observations?. Philos T Roy Soc A, 373, 2052. doi: 10.1098/rsta.2014.0164, 2015

Notz, D., Jahn, A., Holland, M., Hunke, E., Massonet, F., Stroeve, J., Tremblay, B. and Vancoppenolle, M.: The CMIP6 Sea-Ice Model Intercomparison Project (SIMIP): understanding sea ice through climate-model simulations, Geosci. Model Dev., 9, 3427–3446. doi:10.5194/gmd-9-3427-2016, 2016

Olonscheck, D. and Notz, D.: Consistently Estimate Internal Climate Variability from Climate Model Simulations. J. Clim., 30, 23, 9555–9573. doi: 10.1175/JCLI-D-16-0428.1, 2018

Ono, N.: Specific heat and heat of fusion of sea ice. In H. Oura, editor, Physics of Snow and Ice, 1, 599–610. Institute of Low Temperature Science, Hokkaido, Japan, 1967

Perovich, D. and Elder, B.: Estimates of ocean heat flux at SHEBA, Geophys. Res. Lett., 29, 9, 58-1-58-4. doi: 10.1029/2001GL014171, 2002

Perovich, D. and Richter-Menge, J. A.: From points to Poles: extrapolating point measurements of sea-ice mass balance, Ann Glaciol, 44, 188-192. doi: 10.3189/172756406781811204, 2006

Perovich, D., Richter-Menge, J. A., Jones, K. F. and Light, B.: Sunlight, water, and ice: Extreme Arctic sea ice melt during the summer of 2007, Geophys Res Lett, 35, 11. doi: 10.1029/2008GL034007, 2008.

Pirazzini, R.: Factors controlling the surface energy budget over snow and ice, Finnish Meteorological Institute Contributions, 75, 2008.

https://doi.org/10.5194/gmd-2019-113
Preprint. Discussion started: 19 August 2019

Geoscientific Model Development Discussions

Rayner, N. A., Parker, D. E., Horton, E. B., Folland, C. K., Alexander, L. V., Rowell, D. P., Kent, E. C. and Kaplan, A.: Global analyses of sea surface temperature, sea ice, and night marine air temperature since the late nineteenth century. J Geophys Res 108:4407. doi:10.1029/2002JD002670, 2003

Rothrock, D. A., Percival, D. B. and Wensnahan, M.: The decline in arctic sea ice thickness: Separating the spatial, annual, and interannual variability in a quarter century of submarine data. J. Geophys Res (Oceans), 113, C5. doi: 10.1029/2007JC004252, 2008

Schwarzacher, W.: Pack ice studies in the Arctic Ocean. J. Geophys. Res., 64:2357–2367, doi: 10.1029/JZ064i012p02357, 1959.

Semtner, A. J.: A Model for the Thermodynamic Growth of Sea Ice in Numerical Investigations of Climate. J. Phys. Oceanogr., 6, 3, 379–389. doi: 10.1175/1520-0485, 1976.

Stroeve, J. C., Kattsov, V, Barrett, A., Serreze, M., Pavlova, T., Holland, M. M. and Meier, W. N.: Trends in Arctic sea ice extent from CMIP5, CMIP3 and observations. Geophys. Res. Lett., 39, doi: 10.1029/2012GL052676, 2012.

Stroeve, J. C., Barrett, A., Serreze, M. and Schweiger, A.: Using records from submarine, aircraft and satellites to evaluate climate model simulations of Arctic sea ice thickness, The Cryosphere, 8, 1839–1854, doi: 10.5194/tc-8-1839-2014, 2014.

Swart, N. C., Fyfe, J. C., Hawkins, E., Kay, J. E. and Jahn, A.: Influence of internal variability on Arctic sea ice trends, Nat. Clim. Ch., 5, 86–89, doi: 10.1038/nclimate2483, 2015.

Thorndike, A. S., Rothrock, D. A., Maykut, G. A. and Colony, R., The thickness distribution of sea ice, J. Geophys. Res., 80, 4501-4513, doi: 10.1029/JC080i033p04501, 1975

Wang, M. and Overland, J. E.: A sea ice free summer Arctic within 30 years: An update from CMIP5 models. Geophys. Res. Lett., 39, L18501 , doi:10.1029/2012GL052868, 2012

West, A. E., Collins, M. C., Blockley, E., Ridley, J., Bodas-Salcedo, A.: Attribution of sea ice model biases to specific model errors enabled by new induced surface flux framework. The Cryosphere Discuss., https://doi.org/10.5194/tc-2018-60, in review, 2019.

Wettlaufer, J. S.: Heat flux at the ice-ocean interface, J. Geophys Res (Oceans), 96, C4, 7215-7236. doi: 10.1029/90JC00081, 1991

https://doi.org/10.5194/gmd-2019-113
Preprint. Discussion started: 19 August 2019

Geoscientific Model Development Discussions

	Top melt flux		Top conductive flux		Basal conductive flux		Ocean heat flux	
	Mean	Std. dev.	Mean	Std. dev.	Mean	Std. dev.	Mean	Std. dev.
January	0.0	0.0	-19.2	10.3	-13.2	5/9	-0.6	9.0
February	0.0	0.0	-20.0	10.8	-13.6	6.4	-2.2	8.1
March	0.0	0.0	-14.6	7.3	-12.7	4.4	-0.9	8.7
April	0.0	0.0	-5.9	4.4	-9.8	3.3	-0.0	4.9
May	1.3	3.2	0.4	4.0	-6.0	2.2	2.2	4.8
June	16.1	10.1	4.8	3.1	-2.0	1.6	11.0	12.7
July	28.6	16.7	4.4	2.8	0.2	1.3	24.0	24.0
August	7.8	6.4	-1.3	4.9	0.9	0.8	25.1	28.7
September	1.0	1.6	-8.1	7.9	0.4	2.1	11.0	13.5
October	0.0	0.0	-17.2	11.6	-1.9	4.1	3.3	8.8
November	0.0	0.0	-20.8	12.1	-8.5	10.3	3.8	13.4
December	0.0	0.0	-22.3	13.2	-12.4	8.0	-1.0	7.8

Table 1. Mean and standard deviations of fluxes measured from the IMB data in Wm^{-2} in each month of the year. For each flux, the convention is that downwards=positive.

https://doi.org/10.5194/gmd-2019-113
Preprint. Discussion started: 19 August 2019

Geoscientific Model Development Discussions
Open Access
EGU

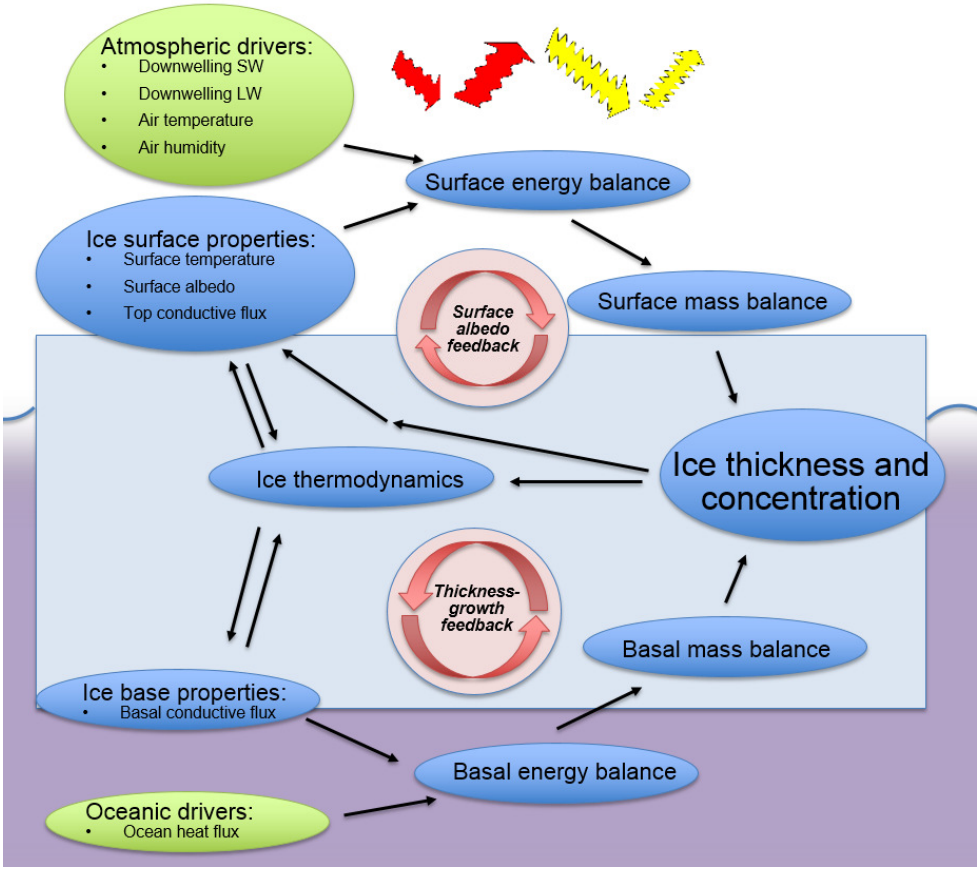

Figure 1. Schematic demonstrating the causal links between ice thickness and extent, and energy and mass balance at the top and basal surfaces of the sea ice.

https://doi.org/10.5194/gmd-2019-113
Preprint. Discussion started: 19 August 2019

Geoscientific Model Development Discussions
Open Access
EGU

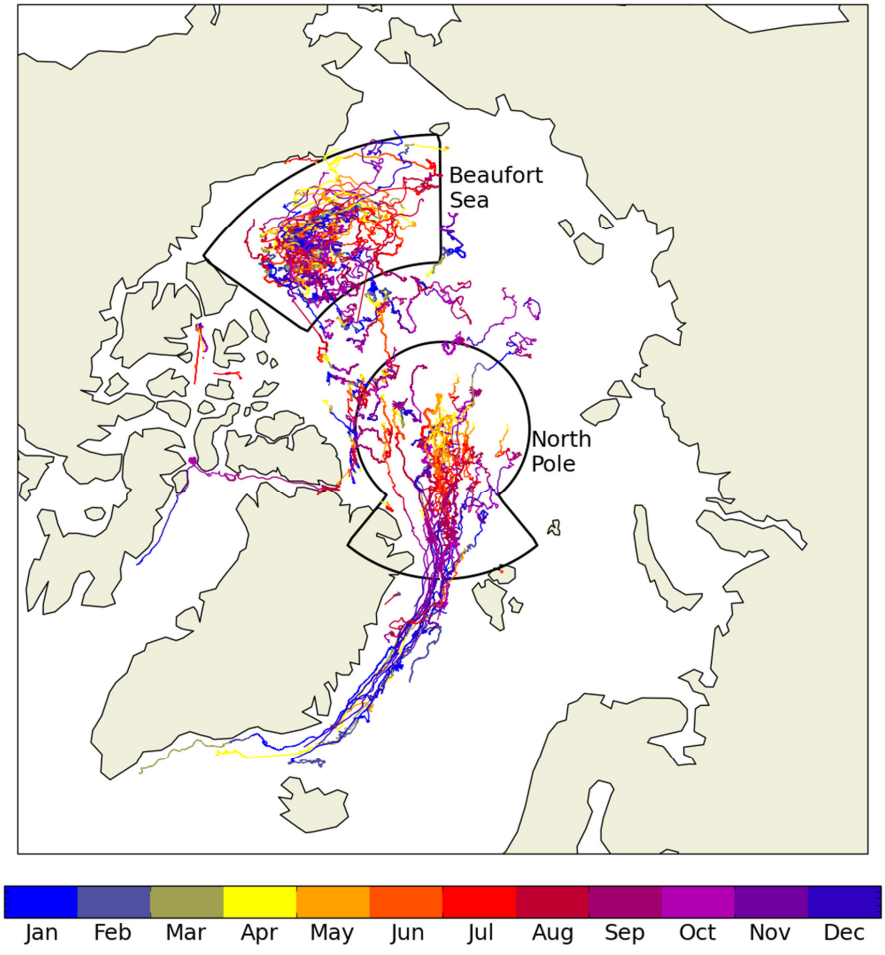

Figure 2. The tracks of Arctic ice mass balance buoys from 1993-2015, with months of coverage indicated by the coloured shading. The North Pole and Beaufort Sea regions used in the analysis are shown by the thin black lines.

https://doi.org/10.5194/gmd-2019-113
Preprint. Discussion started: 19 August 2019

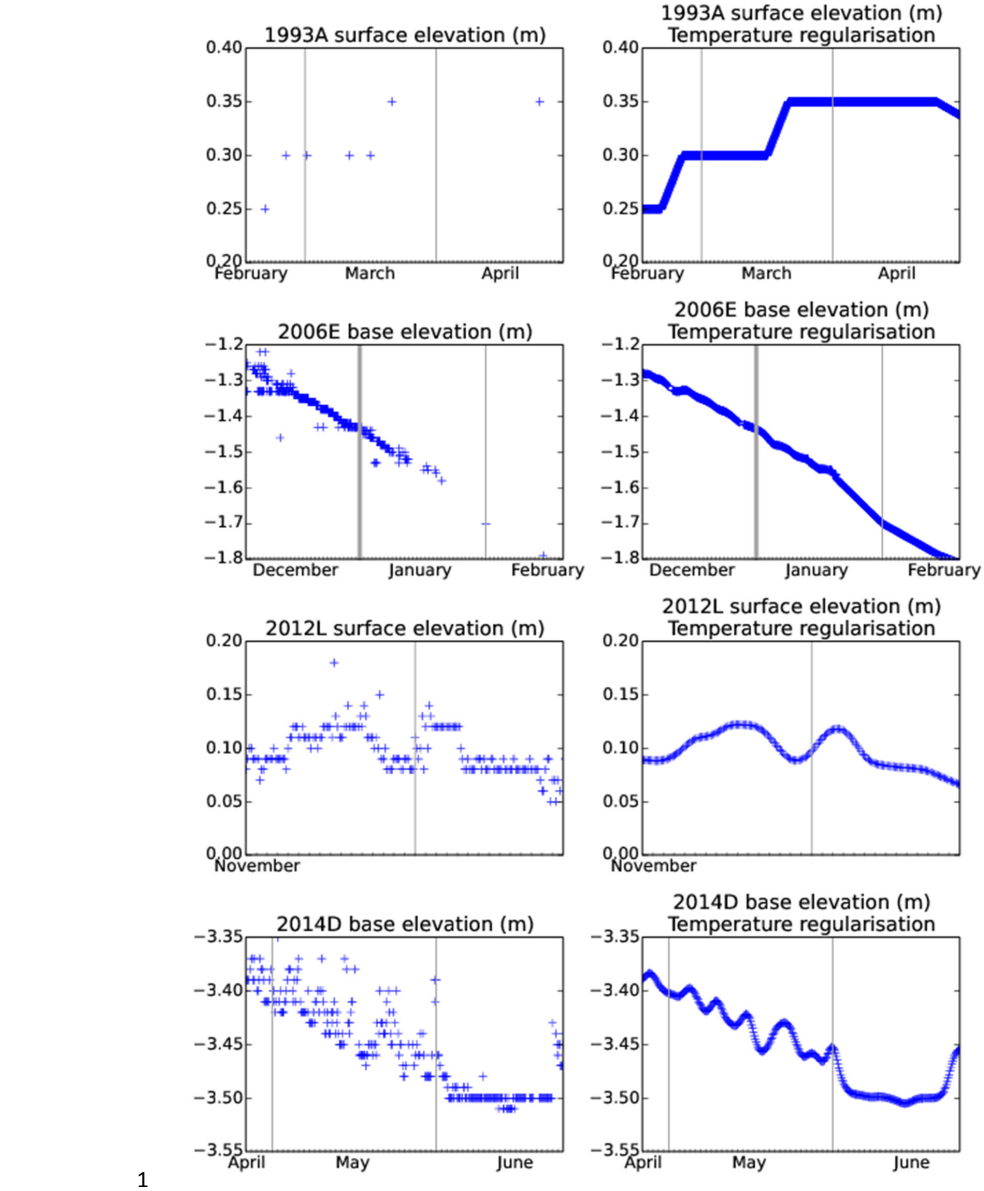

Figure 3. Illustration of the regularisation process using four selected IMB data series. (Left) raw data; (right) temperature regularised time series.

https://doi.org/10.5194/gmd-2019-113
Preprint. Discussion started: 19 August 2019

Geoscientific Model Development Discussions
Open Access
EGU

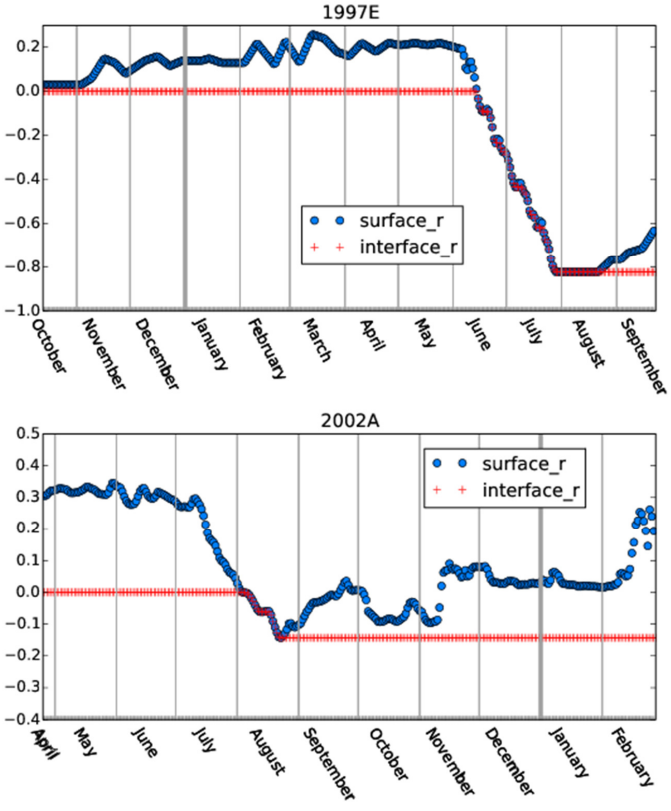

Figure 4. Two examples of estimating snow-ice interface from a regularised snow surface data series. The interface remains at a constant level unless the surface falls below this level, in which case the interface falls with the surface.

https://doi.org/10.5194/gmd-2019-113
Preprint. Discussion started: 19 August 2019

Geoscientific Model Development Discussions
Open Access
EGU

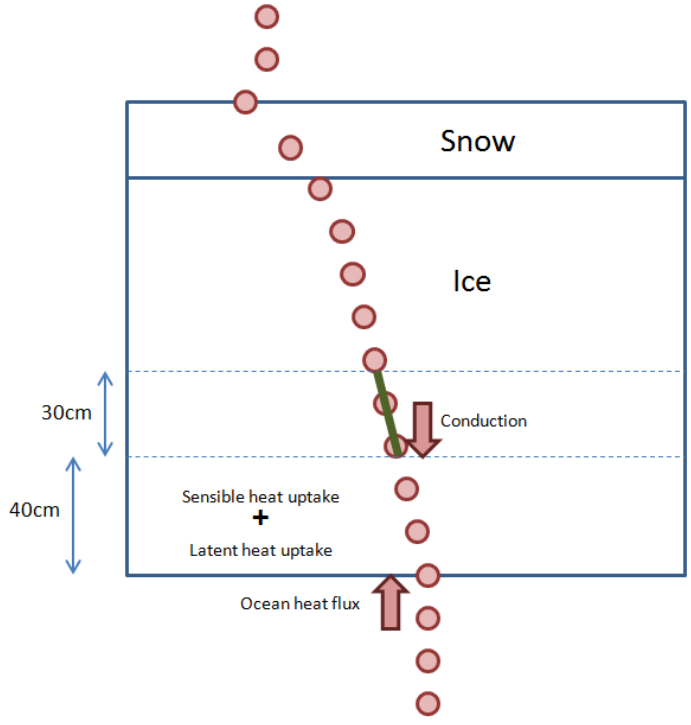

1

2 **Figure 5. Illustrating the calculation of basal conductive flux and ocean heat flux as described in Section**
3 **2, after Lei et al (2014), with the use of a 'buffer zone' in the lowest 40cm of the ice above which the**
4 **conduction is measured.**

https://doi.org/10.5194/gmd-2019-113
Preprint. Discussion started: 19 August 2019

Geoscientific Model Development Discussions
Open Access
EGU

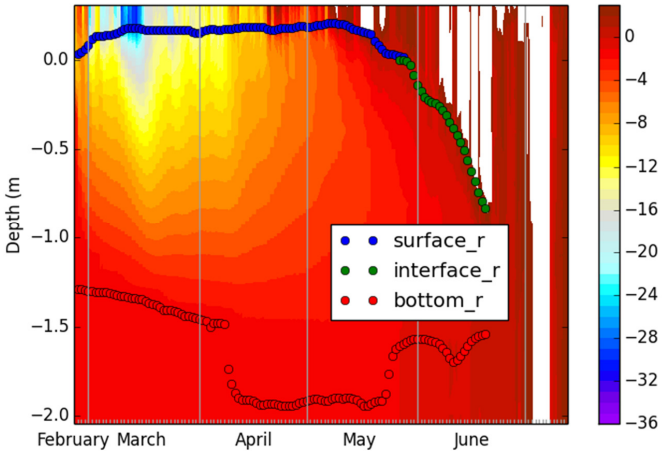

Figure 6. Measurements from the buoy 2015A, with a likely 'false bottom' being measured from early April to late May, characterised by sudden step changes in estimated base elevation.

https://doi.org/10.5194/gmd-2019-113
Preprint. Discussion started: 19 August 2019

Geoscientific Model Development Discussions

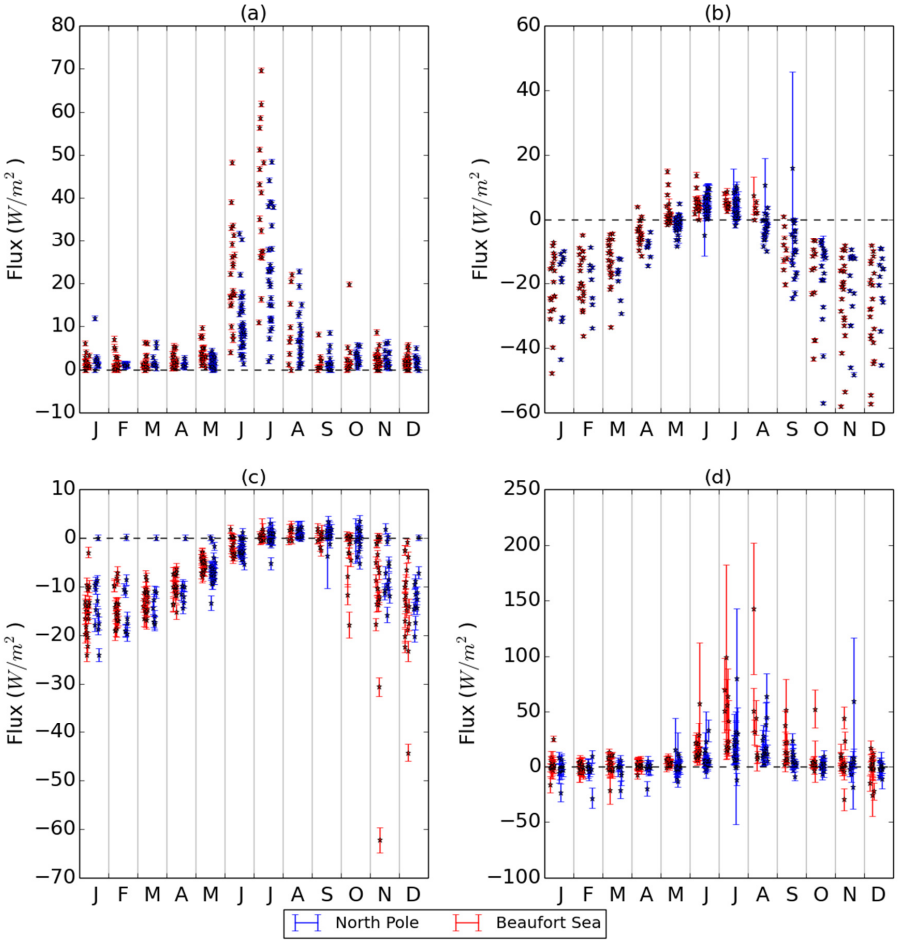

Figure 7. Fluxes of (a) top melting, (b) top conductive flux, (c) basal conductive flux and (d) ocean heat flux, estimated from the IMB data, shown for North Pole (blue) and Beaufort Sea (red) regions. Mean and uncertainty are indicated for each data point. For all fluxes, the convention is that downwards=positive.

https://doi.org/10.5194/gmd-2019-113
Preprint. Discussion started: 19 August 2019

Geoscientific Model Development Discussions

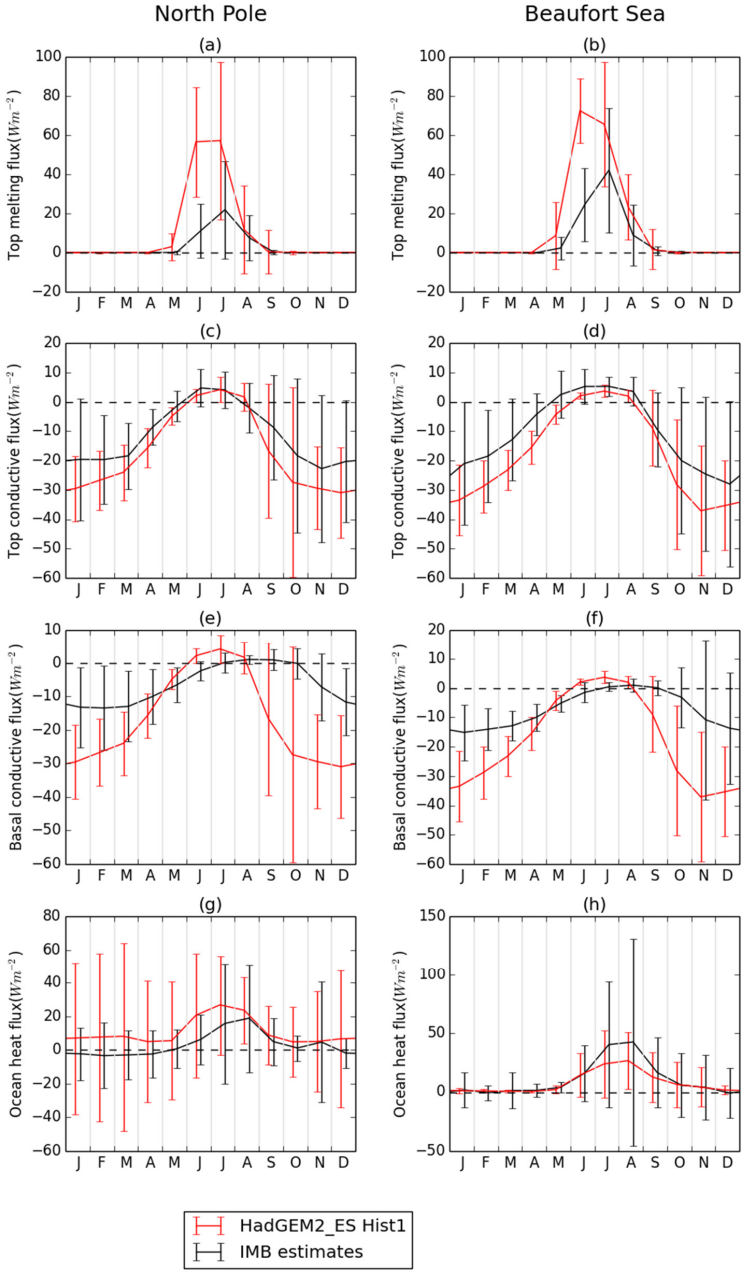

Figure 8. Comparing distributions of (a,b) top melt, (c,d) top conductive flux, (e,f) basal conductive flux and (g,h) ocean heat flux from HadGEM2-ES (red) to those estimated from the IMB data (black), for the North Pole (left) and Beaufort Sea (right) regions.

https://doi.org/10.5194/gmd-2019-113
Preprint. Discussion started: 19 August 2019

Geoscientific Model Development Discussions

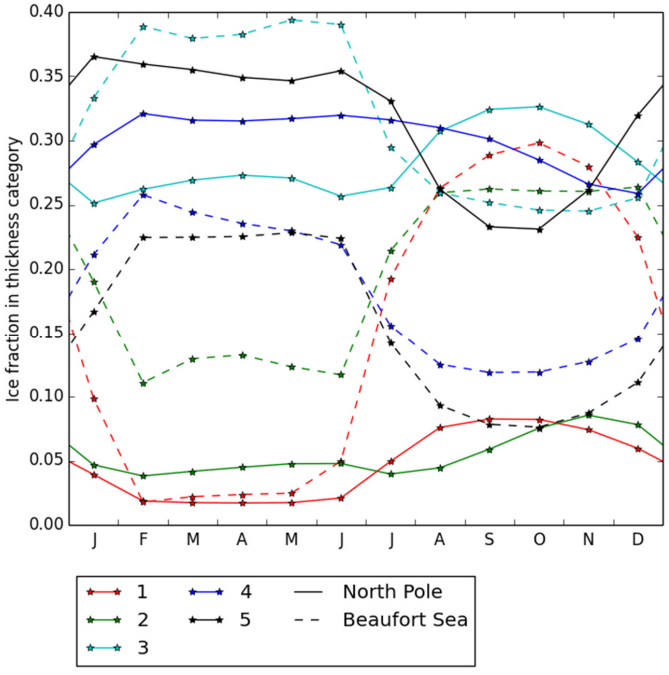

Figure A1. Ice fraction in the 5 thickness categories defined in Appendix A, estimated from submarine data compiled by Rothrock et al. (2008) for the North Pole (solid lines) and Beaufort Sea (broken lines) regions.